Materials Sciences and Applications, **2011, 2, 87-96**
doi:10.4236/msa.2011.22012 Published Online February 2011 (http://www.SciRP.org/journal/msa)

Liquid Column Deformation and Particle Size Distribution in Gas Atomization

Georgios S. E. Antipas

Department of Mining Engineering and Metallurgy National Technical University of Athens Zografou Campus, Athens, Greece.
Email: yantipas@otenet.gr

Received December 22nd, 2010; revised January 5th, 2011; accepted February 12th, 2011.

ABSTRACT

A water-gas flow injected by a close coupled atomizer was studied via High Speed Photography and Phase Doppler Anemometry. The formation of a wave disturbance on the surface of the water column was confirmed. The flow converged within an area approximately 3 mm in diameter, independent of atomization conditions. The particle size distribution across the spray suggested a trend of decreasing particle sizes and particle velocities with increasing distance from the spray axis of symmetry.

Keywords*: *Liquid Column Deformation*, *Two Phase Flow*, *Atomization*, *High Speed Photography*, *Laser Doppler Anemometry

1. Introduction

During close coupled atomization, a liquid column or sheet is perturbed by a high velocity gas flow and is broken up into droplets, in a two stage process. In the first stage, that of primary atomization [1], the surface of the melt is disturbed by a sinusoidal oscillation [2] and is subsequently broken up into large drops or unstable bodies, the ligaments [3]. During the subsequent stage of secondary atomization, the drops/ligaments may further disintegrate in flight, either via a low-turbulence mechanism [4] or in a more chaotic high-turbulence stripping fashion [5]. The principle of gas atomization is shown in **Figure 1**. In spray forming, atomization of a molten metal or alloy causes rapid solidification of the drops in flight. The spray's subsequent impingement on a substrate produces a spray cast of varying microstructure. It is in fact the localized size distribution of particle diameters inside the spray, which dictates the spray cast microstructure and mechanical properties. In turn, local size distributions depend on the break up mechanisms. The latter, have received considerable attention in earlier phenomenological studies [4-14] in respect to atomization parameters – such as nature of the gas and melt phase, gas injection pressures and melt superheat. More recently, experimental treatises of atomizing geometries have been presented [15-16]. Liquid break up phenomena, however – although described in the macro scale early on (e.g. [17-20]) – have not been reflected on rigorous modeling implementations. Modern atomization modeling ap-

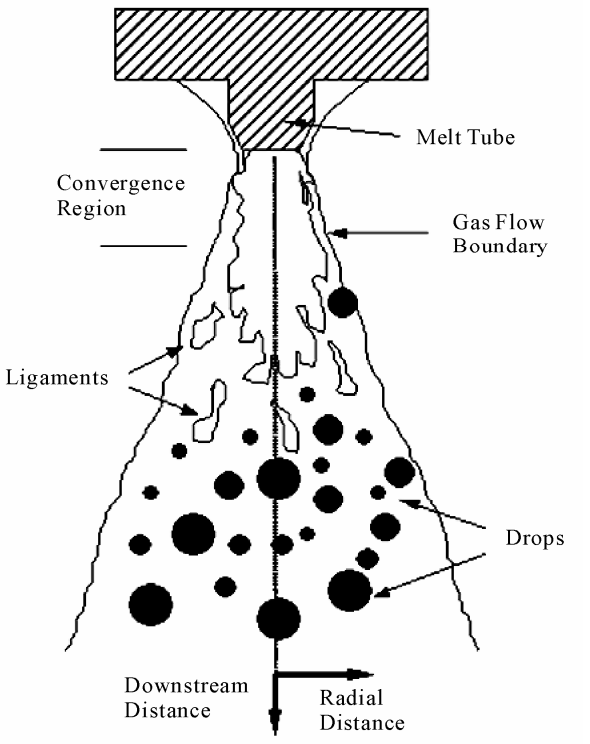

Figure 1. The principle of atomization.

pears to be focusing on CPU-intensive stochastic simulation of the liquid jet and primary atomization in terms of Reynolds- averaged Navier-Stokes mixing (e.g. [21]). Recently, the more realistic cases of turbulent atomization conditions have been addressed – e.g. by CFD (see [22-24]) and integrated models [15] have been proposed.

The current study investigates the initial stage of turbulent mixing in a close coupled atomizer, which is assumed to take place within a finite convergence region; this region constitutes a crucial subtlety of a flexible mathematical model for the atomization of liquid metals already presented elsewhere [25]. The model - covering both primary and secondary atomization - is applicable to any liquid//gas system and is based on the formation of sinusoidal traveling waves along the surface of a liquid [26,27]. Estimation of the convergence region diameter is of great importance to modeling of the gas flow [28], as it determines the Mach number, static temperature and sonic velocities of the gas inducing break up of the liquid column.

2. Experimental Procedure

A cross section of the close coupled assembly used in this study is shown in **Figure 2**. The atomizer consisted of 20 gas jets arranged in a ring configuration. Each jet outlet diameter was 0.75 mm and its each inclination from the vertical direction was 20˚.

2.1. High Speed Photography

The behavior of a water column perturbed by Nitrogen and Helium gases was studied. The choice of water as the atomized medium was due to its low viscosity, which in turn was expected to lead to the formation of larger surface wave amplitudes for a given gas velocity, as outlined in [25]. An Imacon 790 high speed camera fitted with a Nikon micro-Nikkor 55 mm lens was used; the camera was capable of speeds ranging between 104 and 107 frames per second. An intermediate tube of 21 mm between the lens and the aperture offered a fixed magnification of × 1.5. The diameter of the water column was either 2 or 3 mm. The experiments were conducted in ambient pressure (0.1 MPa) and temperature (17˚C). The high speed frames presented in this study are based on original photographs in which the contrast between the actual water column and the background has been enhanced by means of response curve filtering. The experimental assembly used in the high speed photography studies is shown in **Figure 3**.

2.2. Phase Doppler Anemometry (PDA)

The dynamic history of moving water particles during atomization was studied by a Dantec Particle Dynamics Analyser. The system is based on the Phase Doppler principle for non-intrusive real time measurements of a wide range of particle sizes. An Ar-ion laser with a maximum output of 5 W was employed, capable of measuring particles in the range of 1-1000 μm over 1.2 m away from the source with an error of 4%. The maximum measurable velocity was 500 m/s with an error of 1%. The output included the mean and turbulent components of particle velocities in the downstream and radial direction of the flow, the mass flux inside the measurement volume and a number of characteristic mean diameters such as the D_{32} (Sauter) particle size. The disintegration of a water column 3 mm in diameter atomized by Nitrogen, Argon and Helium gases at a pressure of 100 psi (0.68 MPa) was studied. A fixed 70˚ angle was main-

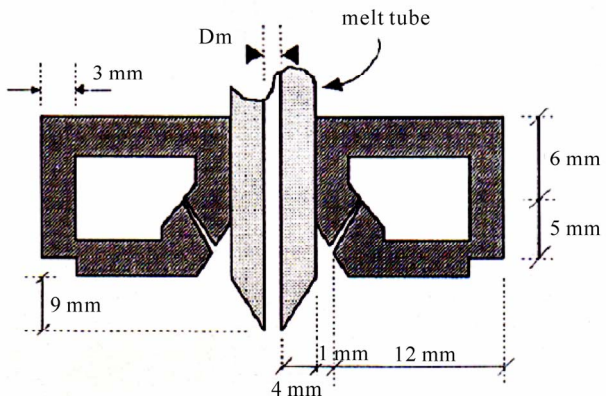

Figure 2. Geometry of the close coupled atomizer.

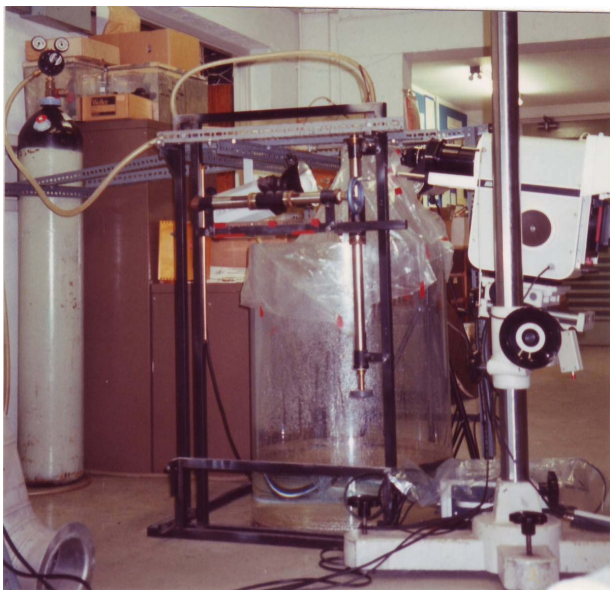

Figure 3. High speed photography assembly.

tained between the laser source and the detector. A fixed horizontal spacing of 600 mm was kept between the detector and the point of convergence of the individual laser beams. The Phase Doppler apparatus used in this study is shown in **Figure 4**.

3. Results and Discussion

3.1 High Speed Photography

The flow was studied between the tip of the melt tube and approximately 12 mm below the melt tube.

Atomization and complete disintegration of the water column was found to depend strongly on the velocities of the two phases. With reducing initial water velocity, break up of the column was more complete further upstream. A low water velocity amounts to a high relative velocity between the melt and gas phase and a correspondingly high growth rate of the surface disturbance [25]. Higher growth rates also mean that the time required for the instability to acquire sufficiently large amplitudes is relatively large and as a result, the break up length of the jet is correspondingly decreased. **Figures 5(a)** and **(b)** give supporting evidence. In the case of water issuing from the delivery tube at a velocity of 7 m/s atomized by Nitrogen at 20 psi (0.14 MPa), the conical spray jet is formed at the tip of the tube – see **Figure 5(a)** – while at a higher water velocity of 13 m/s - e.g. **Figure 5(b)** – there is an unbroken core of water 6 mm in length before the formation of the spray cone. At sufficiently high melt velocities and at relatively low gas pressures the column exhibited a tendency for sinusoidal antisymmetric oscillations, as shown in **Figure 5(c)**.

Superimposed on the antisymmetric mode, oscillations of the symmetric type, as shown in **Figure 5(d)** gave rise to the formation of crests which normally led to the detachment of fragments from the disturbed column surface, shown in **Figure 5(e)**. The symmetric instability amplitudes were an order of magnitude smaller than those of the antisymmetric type. An increase in the diameter of the water column caused a reduction in the wavelengths disturbing the surface of the water column. This in turn led to the disintegration of the column further downstream from the point of initial atomization.

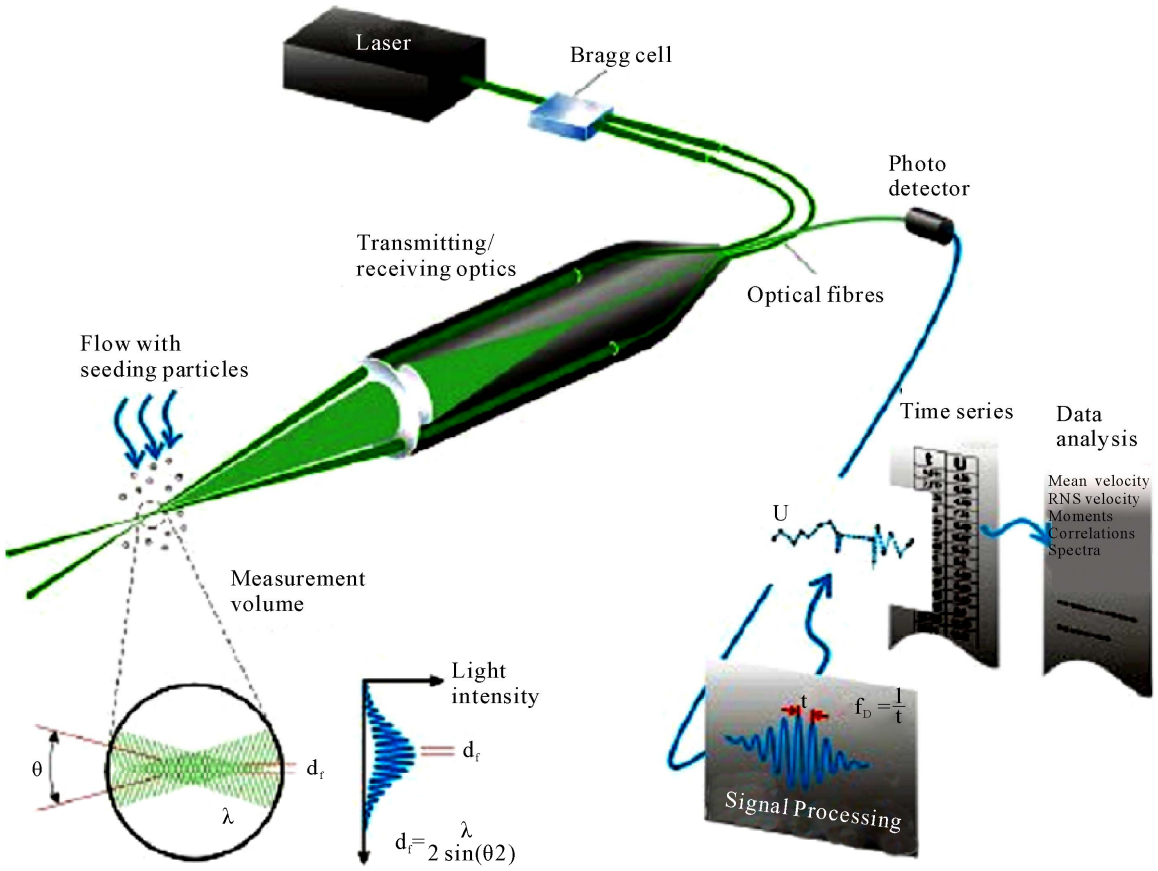

Figure 4. Phase Doppler Anemometry apparatus.

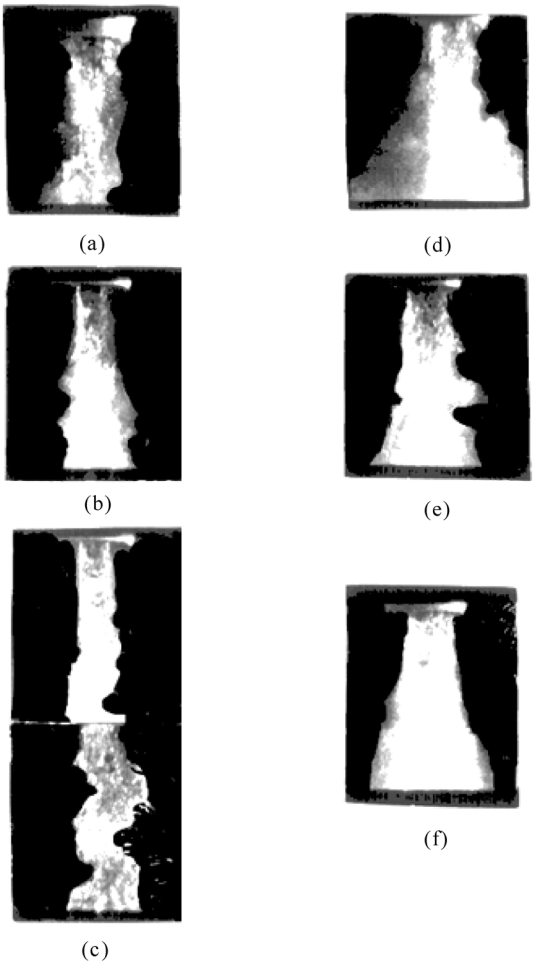

Figure 5. (a) Water (2 mm) at 7 m/s, N_2 at 20 psi, 2.5 * 104 frames/s; (b) Water (2 mm) at 13 m/s, N_2 at 20 psi, 2.5 * 104 frames/s; (c) Water (2 mm) at 13 m/s, N_2 at 10 psi, 2.5 * 104 frames/s; (d) Water (2 mm) at 13 m/s, He at 50 psi, 105 frames/s; (e) Water (3 mm) at 7 m/s, N_2 at 30 psi, 106 frames/s; (f) Water (3 mm) at 7 m/s, N_2 at 30 psi, 105 frames/s.

Formation of a conical spray jet a certain distance below the point of convergence of the gas jets was always a predominant feature. This seemingly uniform spray jet initiated approximately 5 mm downstream from the tip of the water delivery tube for any set of experimental parameters. The angle of the jet was constant and roughly equal to 20˚ as long as turbulent conditions for the gas phase were satisfied – see **Figure 5(f)**. In general, no crest observed reached amplitude greater than the water column radius. The diameter of the convergence region, taken to be the point at which the spray jet appeared to have the smallest diameter, was also measured on every photograph and was found to be equal to a constant value of 3 mm. This diameter was found to be independent of the radius of the water column, the type of atomizing gas and the injection pressure.

3.2. Phase Doppler Anemometry

In the water sprays examined by PDA, the radial distribution of drops 40 mm downstream from the tip of the melt tube was always found to be irregular. **Figures 6(a)**, **(b)** and **(c)**, for Nitrogen, Argon and Helium flows respectively, suggest that the coarser fragments of the spray lie in close proximity of the central axis, defined as the point of maximum flux and their diameter decreases with increasing distance from the central axis. The assumption of maximum particle flux along the centre axis

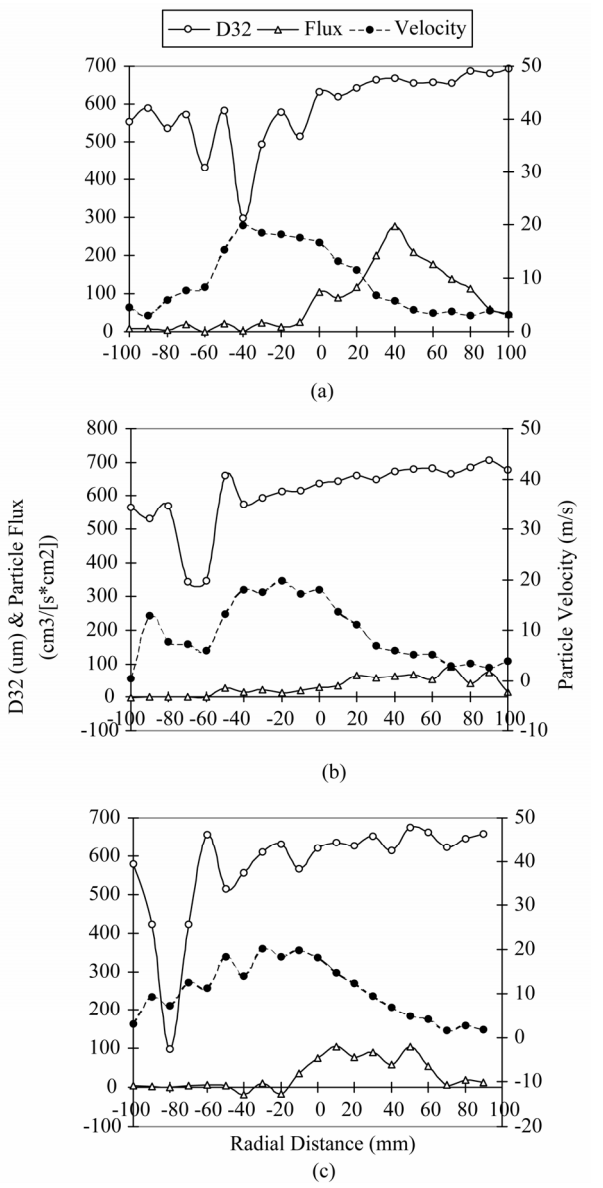

Figure 6. Radial distribution of particle size, velocity and volume flux for water atomized by: (a) N_2 at 50 psi (0.34 MPa); (b) Ar at 50 psi; (c) He at 50 psi.

of the spray has been experimentally confirmed by spray forming experiments of Al alloys [29]. In addition, it has been shown that particle sizes monotonically decrease with distance from the centre of the flow [25]. The profiles in **Figure 6** may appear asymmetric due to the mismatch between the vertical axis of motion of the PDA apparatus and the actual vertical axis of symmetry of the spray. It is unlikely that the two axes can be made to overlap, due to the highly turbulent nature of the flow which causes the spray's axis of symmetry to fluctuate. The largest measured diameters produced by Nitrogen and Argon, **Figures 6(a)** and **(b)** respectively, were of the order of 700 μm, while Helium, as shown in **Figure 6(c)**, produced finer particles. Numerical data underlying to **Figure 6** are presented in, **Table 1**.

Variation of the D_{32} particle size and the mean downstream particle velocity as a function of distance from the point of initial atomization are shown in **Figures 7(a)** and **(b)**, for Nitrogen and Argon respectively. Comparison of the two plots suggests that the spray in its infancy contained globules of diameter 550 μm in the case of Nitrogen and 600 μm in the case of Argon. The nature of the gas did not substantially influence the products of primary atomization at this pressure, since the initial drop diameters for both flows were quite similar. It is possible that the primary particles formed during the disintegration of the melt column were even larger in diameter. This is suggested by the fact that the PDA technique cannot accurately measure drop sizes upstream a 50 mm distance from the tip of the melt tube, as **Figure 7(a)** indicates. Break up of the water particles was complete within 150 mm downstream of the point of initial atomization, resulting in a spray that consisted of particles 100 μm in diameter. In the case of Argon, completion of break up as a slight change in the D_{32} slope could be distinguished at approximately 200 mm below the die. The overall reduction in diameters for the Nitrogen flow was 80% while in the case of Argon it was 65%. These figures, however, are by no means indicative of the atomization efficiency of the configuration, since they only serve as a comparison between the fragments of primary and secondary break up. In general, the velocity followed the inverse trend of the particle size, *i.e.* in the early atomization stages fragments decreased in size whilst gaining in velocity. After completion of the break up

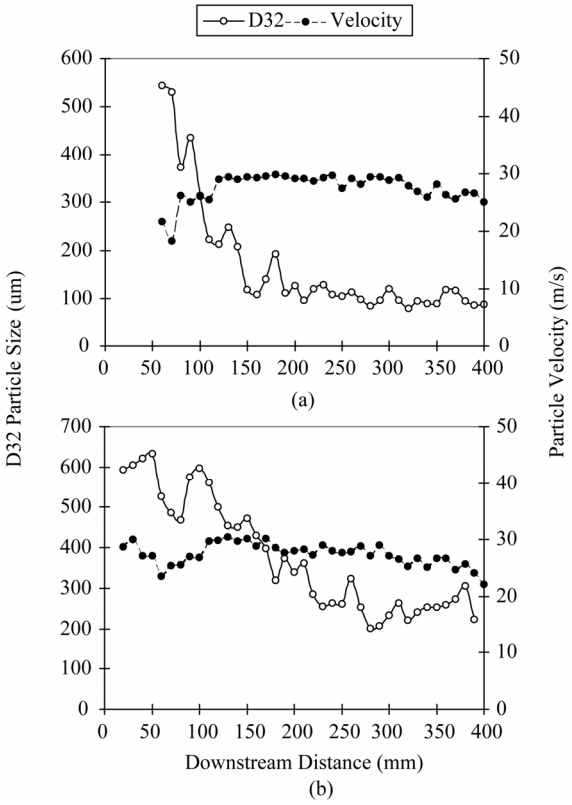

Figure 7. Variation of particle velocities along the center axis for water atomized by: (a) N_2 at 100 psi (0.68 MPa); (b) Ar at 100 psi.

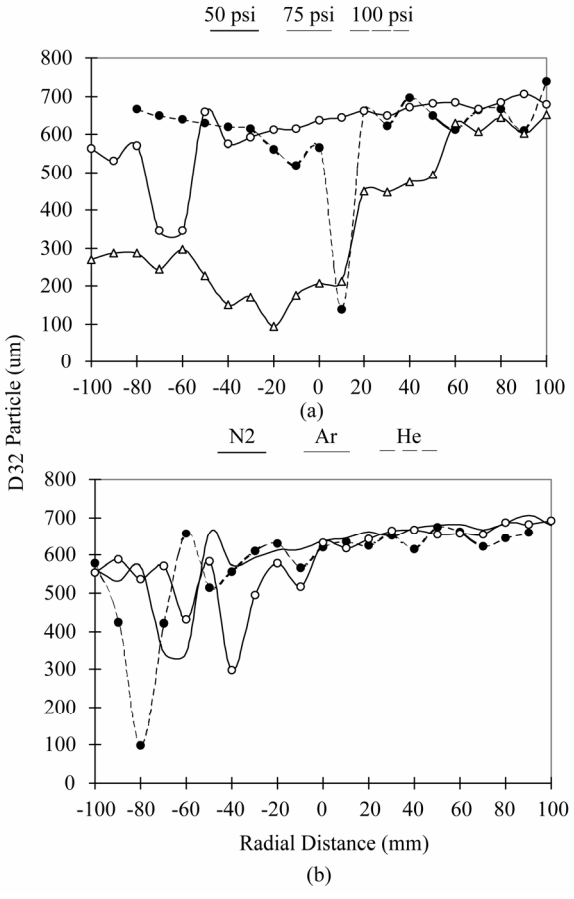

Figure 8. (a) Effect of the injection pressure of Ar on the radial variation of the D_{32} size; (b) Effect of type of atomizing gas on the radial variation of the D_{32} size.

Table 1. Particle size, velocity and volume flux for water atomized at 50 psi (0.34 MPa).

	Nitrogen			Argon			Helium		
Radial distance (mm)	Velocity (m/s)	D_{32} (μm)	Flux ($cm^3/s * cm^2$)	Velocity (m/s)	D_{32} (μm)	Flux ($cm^3/s * cm^2$)	Velocity (m/s)	D_{32} (μm)	Flux ($cm^3/s * cm^2$)
−100	4.609	554.2	7.482	0.397	564.2	−1.143	3.053	579.1	5.395
−90	3.016	588.7	8.886	12.829	531.6	0.667	9.223	422.7	2.493
−80	5.946	537	4.972	7.782	569.2	1.222	7.276	98.79	0.017
−70	7.707	571.8	18.563	7.228	345.1	0.652	12.563	421.4	4.59
−60	8.308	431.3	0.737	5.949	345.7	0.374	11.297	656.1	6.518
−50	15.363	583	20.503	13.164	660.3	27.612	18.361	514.7	4.274
−40	19.927	298.2	2.406	18.035	574.4	15.101	13.978	555.9	−18.754
−30	18.534	493.8	22.55	17.596	592.8	23.36	20.3	611	11.38
−20	18.286	578.5	12.516	19.739	612.1	13.564	18.464	630.5	−15.865
−10	17.651	515.8	24.898	17.177	614.4	20.185	19.923	565.4	35.828
0	16.736	632	104.02	18.058	637.8	29.867	18.153	621.4	75.328
10	13.271	618.3	89.053	13.686	645	33.475	14.746	634.5	105.015
20	11.494	642.1	117.685	11.1	661.5	65.545	12.318	625.9	76.575
30	6.869	664.8	198.979	6.956	649.3	57.443	9.341	652.5	89.29
40	5.738	667.2	276.583	5.942	672.8	63.682	6.804	615.3	58.847
50	4.178	655.2	208.98	5.247	680.6	67.619	4.884	675.5	104.651
60	3.561	657	176.506	5.219	682.8	52.473	4.212	662.9	54.669
70	3.766	655	138.849	2.999	666.4	90.94	1.541	623.5	7.183
80	3.078	687.4	113.705	3.501	684	42.072	2.585	646	18.388
90	3.919	681.3	59.745	2.598	705.8	75.618	1.739	658.6	13.604
100	3.163	692.6	46.703	3.953	678.5	15.569			

process (e.g. 200 mm in the case of water/Nitrogen, see **Figure 7(a)** the velocities remained constant within a limited distance and started decaying from that point downstream. Numerical data underlying to **Figure 7** are presented in, **Table 2**.

The effect of the atomizing pressure on the particle size distribution inside the flow, in the case of Argon, is shown in **Figure 8(a)**. D_{32} decreased in all regions of the spray with increasing injection pressure of the gas phase. The primary fragments (in the centre of the spray) were not substantially affected by the change in injection pressure, while the fragments on the flow edge decreased in size. At 50 psi (0.34 MPa) the majority of the spray, lying in the outer 16o of the spray cone, was made up by particles in the region of 650 μm. The inner region of the cone, within an angle of 4o from the centre axis, contained particles approximately 50% smaller compared to the rest of the spray. At 75 psi (0.52 MPa) there was a wide variety of sizes along the radial direction, ranging from primary fragments in the centre of the flow, to the finer by 80% particles on the spray edge, the latter being finer than the ones at the same point produced at a pressure of 50 psi (0.34 MPa). At an injection pressure of 100 psi (0.69 MPa) the diameter of the larger particles in the centre of the flow was reduced while the size of the finest particles was not affected. The mean particle size and the distribution of diameters in the spray were greatly dependent on the type of the atomizing gas. A comparison of the diameters produced by Nitrogen, Argon and Helium, is shown in **Figure 8(b)**, where the injection pressure of the gas was 50 psi (0.34 MPa). All types of gases produced similar primary fragments that covered most of the spray area. Nitrogen and Argon produced the largest particles whilst Helium yielded 25% finer particles along

Table 2. Particle size and velocity for water atomized at 100 psi (0.68 MPa).

	Nitrogen		Argon	
Downstream Distance (mm)	D_{32} (μm)	Velocity (m/s)	D_{32} (μm)	Velocity (m/s)
0				
10				
20			593.588	28.697
30			604.923	30.053
40			621.754	27.211
50			632.666	27.093
60	544.833	21.675	526.565	23.551
70	531.433	18.286	486.413	25.384
80	373.715	26.177	468.743	25.546
90	436.078	25.095	575.132	27.055
100	313.379	26.176	596.728	26.912
110	223.32	25.545	561.224	29.751
120	213.557	29.024	501.027	29.857
130	248.314	29.399	455.383	30.491
140	208.515	29.026	450.582	29.678
150	117.699	29.411	472.545	30.128
160	108.976	29.299	429.566	28.851
170	140.312	29.563	398.381	30.137
180	193.437	29.922	319.572	28.601
			374.255	27.774
210	95.953	29.158	361.140	28.376
220	120.225	28.747	285.585	27.313
230	128.376	29.242	256.276	29.007
240	107.711	29.749	263.700	27.991
250	104.118	27.507	261.941	27.704
260	113.444	29.225	322.845	27.855
270	97.457	28.187	253.981	28.875
280	84.317	29.467	200.456	27.089
290	96.488	29.468	207.036	28.986
300	119.16	28.846	234.194	27.088
310	96.471	29.329	262.674	26.515
320	79.099	27.939	221.533	25.216
330	94.125	26.964	241.347	26.66
340	89.702	25.862	252.457	25.087
350	89.6	28.215	253.982	26.716
360	118.154	26.308	258.658	26.684
370	116.628	25.67	273.361	24.693
380	94.316	26.784	306.736	25.681
390	85.658	26.584	224.107	24.143
400	87.688	25.123		22.105

the central axis of the spray, compared to Nitrogen and Argon. Numerical data underlying to **Figure 7** are presented in, **Table 3**.

The effect of the injection pressure on the distribution of particle velocities is shown in **Figure 9(a)**, in the case of Argon. The mean components of the downstream velocities were normalized by the component measured on the theoretical centre axis of the spray for the flow generated by Argon at 100 psi (0.69 MPa). The general trend suggests that the particle velocities increase with decreasing distance from the real axis of symmetry of the spray and with increasing atomization pressure. Every 50 psi (0.34 MPa) increase in injection pressure seems to result in a 20% increase in the maximum velocity of the distribution. **Figure 9(b)** indicates that the type of atomizing gas does not affect the particle velocities substantially. Numerical data underlying to **Figure 9** are presented in, **Table 4**.

4. Conclusions

High Speed Photography studies of the area of the spray

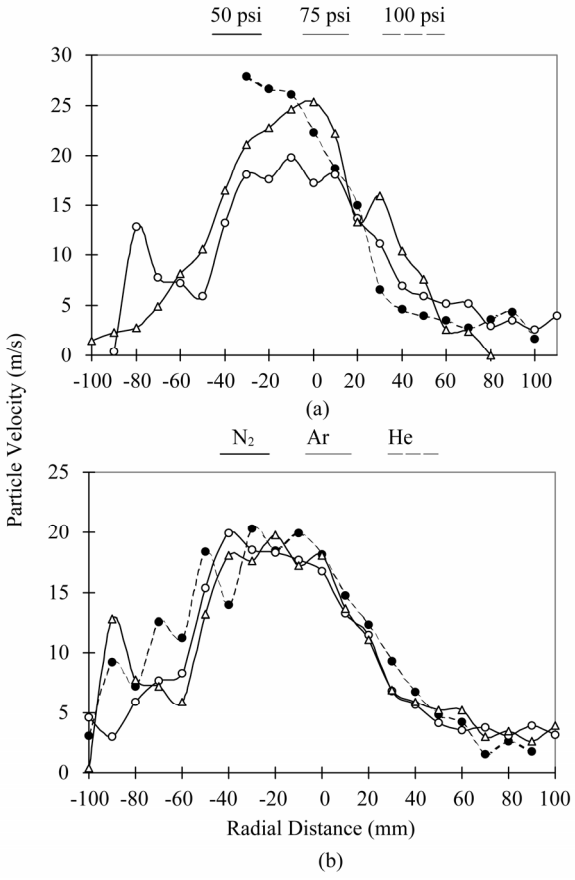

Figure 9. (a) Effect of the injection pressure of Ar on the radial variation of particle velocity; (b) Effect of type of atomizing gas on the radial variation of particle velocity.

Table 3. Effect of injection pressure and type of atomizing gas on particle size.

	Nitrogen			50 psi		
Radial Distance (mm)	50 psi	75 psi	100 psi	Nitrogen	Argon	Helium
−100	0.397	1.461		4.609	0.397	3.053
−90	12.829	2.352		3.016	12.829	9.223
−80	7.782	2.794		5.946	7.782	7.276
−70	7.228	4.936		7.707	7.228	12.563
−60	5.949	8.193		8.308	5.949	11.297
−50	13.164	10.629		15.363	13.164	18.361
−40	18.035	16.441		19.927	18.035	13.978
−30	17.596	21.057	27.859	18.534	17.596	20.3
−20	19.739	22.776	26.7	18.286	19.739	18.464
−10	17.177	24.612	26.136	17.651	17.177	19.923
0	18.058	25.4	22.268	16.736	18.058	18.153
10	13.686	22.165	18.669	13.271	13.686	14.746
20	11.1	13.243	14.916	11.494	11.1	12.318
30	6.956	15.894	6.606	6.869	6.956	9.341
40	5.942	10.366	4.659	5.738	5.942	6.804
50	5.247	7.57	4	4.178	5.247	4.884
60	5.219	2.637	3.542	3.561	5.219	4.212
70	2.999	2.413	2.749	3.766	2.999	1.541
80	3.501	0.042	3.597	3.078	3.501	2.585
90	2.598		4.372	3.919	2.598	1.739
100	3.953		1.666	3.163	3.953	

close to the tip of the melt delivery tube on a close-coupled atomizer for a water-gas spray, indicated that at sufficiently high melt exit velocities and at relatively low atomization gas pressures the water column was deformed by sinusoidal antisymmetric oscillations. Symmetric oscillations that were superimposed on the antisymmetric mode had amplitudes about an order of magnitude smaller than those of the antisymmetric type. No crest, formed on the surface of the water column during the process of primary break up, was observed to reach an amplitude greater than roughly half the diameter of the water column. An increase of the diameter of the water column seemed to cause a reduction in the wavelengths disturbing its surface and the subsequent breakdown of the column. The use of Helium as the atomizing medium was found to cause the disintegration of the water column further upstream compared to Nitrogen. In addition, what looked like an unbroken core of water covered by dense spray, initiating from the tip of the melt delivery tube, was always shorter for the Helium than for the Nitrogen atomization runs. The diameter of the convergence region was found to be equal to 3 mm and was not affected by the gas injection pressure or the melt flow rate.

PDA measurements of the particle size and velocity in the water/gas jet indicated that the particle size decreases with increasing distance from the centre axis. Measurements of drop sizes along the centre axis of the flow indicated that break up was complete at a downstream distance of 150 to 200 mm from the die. Helium produced the finest particles and the highest particle velocity compared to Nitrogen and Argon. The radial distribution of particle size was sensitive to changes in the injection pressure of the gas but was not affected by the type of gas. As a general rule the velocities of the particles in the flow were not sensitive to the gas pressure or the nature

Table 4. Effect of injection pressure and type of atomizing gas on particle velocity.

	Nitrogen			50 psi		
Radial Distance (mm)	50 psi	75 psi	100 psi	Nitrogen	Argon	Helium
−100	564.164	269.102		554.217	564.164	579.054
−90	531.587	286.673		588.707	531.587	422.689
−80	569.249	285.843	666.897	537.049	569.249	98.789
−70	345.137	245.258	650	571.783	345.137	421.375
−60	345.739	295.274	640	431.27	345.739	656.091
−50	660.251	226.992	630	582.973	660.251	514.699
−40	574.352	151.418	620	298.166	574.352	555.862
−30	592.781	170.734	614.405	493.848	592.781	611.016
−20	612.055	93.579	560	578.485	612.055	630.541
−10	614.374	174.542	517.619	515.82	614.374	565.442
0	637.826	208.524	566.447	631,966	637.826	621.402
10	645.004	211.822	138.862	618.253	645.004	634.517
20	661.508	450.575	660.894	642.143	661.508	625.893
30	649.298	445.947	623.267	664.796	649.298	652.534
40	672.778	472.901	697.247	667.218	672.778	615.272
50	680.584	493.555	650	655.248	680.584	675.549
60	682.835	630.771	612.531	656.987	682.835	662.894
70	666.44	606.578	664.22	655.005	666.44	623.471
80	684.008	645.132	665.866	687.355	684.008	646.001
90	705.803	602.265	611.01	681.273	705.803	658.556
100	678.458	652.001	737.323	692.584	678.458	

of the gas phase.

REFERENCES

[1] C. Dumouchel, J. Cousin and K. Triballier, "Experimental Analysis of Liquid-Gas Interface at Low Weber Number: Interface Length and Fractal Dimension," *Experiments in Fluids*, Vol. 39, No. 4, 2005, pp. 651-666. doi:10.1007/s00348-005-1005-5

[2] L. Fei, S. Xu and S. Huang, "Relaxation and Breakup of a Cylindrical Liquid Column," *Science in China Series E*: *Technological Sciences*, Vol. 51, No. 2, 2008, pp. 145-152. doi:10.1007/s11431-008-0018-8

[3] J. Shinjo and A. Umemura, "Simulation of Liquid Jet Primary Breakup: Dynamics of Ligament and Droplet Formation," *International Journal of Multiphase Flow*, Vol. 36, No. 7, 2010, pp. 513-532. doi:10.1016/j.ijmultiphaseflow.2010.03.008

[4] C. L. Ng, R. Sankarakrishnana and K. A. Sallam, "Bag Breakup of Nonturbulent Liquid Jets in Crossflow," *International Journal of Multiphase Flow*, Vol. 34, No. 3, 2008, pp. 241-259.

[5] D. R. Guildenbecher, C. López-Rivera and P. E. Sojka, "Secondary Atomization," *Experiments in Fluids*, Vol. 46, No. 3, 2009, pp. 371-402. doi:10.1007/s00348-008-0593-2

[6] M. Arai, M. Shimizu and H. Hiroyasu, "Break-up Length and Spray Formation Mechanism of a High Speed Liquid Jet," *Proceedings of the International Conference of Liquid Atomization and Spray Systems* (*ICLASS*-88), London, 1988, pp. 177-184.

[7] H. Hiroyasu, M. Shimizu and M. Arai, "The Breakup of a High Speed Jet in a High Pressure Gaseous Atmosphere," *Proceedings of the International Conference of Liquid Atomization and Spray Systems* (ICLASS-82), Madison, 1982, pp. 69-74.

[8] R. Ingebo, "Experimental and Theoretical Effects of Nitrogen Gas Flow Rate on Liquid-Jet Atomization," *Jour-*

nal of Propulsion and Power, Vol. 4, No. 5, 1988, pp. 406-411.
doi:10.2514/3.23081

[9] M. Kim and H. Jones, "Effect of Process Variables in Gas-Jet Atomization and Production of Multilayer Deposits," *Proceedings of the Fourth International Conference on Rapidly Quenched Metals*, Sendai, 1981, pp. 85-88.

[10] B. Pai and B. Nijaguna, "The Charecterization of Sprays," *International Conference on Liquid Atomization and Spray Systems*, Madison, 1982, pp. 29-35.

[11] R. Reitz, "Modeling Atomization Processes in High-Pressure Vaporizing Sprays," *Atomization and Spray Technology*, Vol. 3, No. 4, 1987, pp. 309-337.

[12] J. See and G. Johnston, "Interactions between Nitrogen Jets and Liquid Lead and Tin Streams," *Powder Technology*, Vol. 21, No. 1, 1978, pp. 119-133.
doi:10.1016/0032-5910(78)80115-6

[13] A. Ünal, "Effect of Processing Variables on Particle Size in Gas Atomization of Rapidly Solidified Aluminium Powders," *Materials Science and Technology*, Vol. 3, 1987, pp. 1029-1039.

[14] S. Zanelli, "Behaviour of a Liquid Jet near the Nozzle," *International Conference on Liquid Atomization and Spray Systems*, 1988, pp. 1-14.

[15] C. Dumouchel, "On the Experimental Investigation on Primary Atomization of Liquid Streams," *Experiments in Fluids*, Vol. 45, No. 3, 2008, pp. 371-422.
doi:10.1007/s00348-008-0526-0

[16] B. Vukasinovic, M. K. Smith, and A. Glezer, "Mechanisms of Free-Surface Breakup in Vibration-Induced Liquid Atomization," *Physics of Fluids*, Vol. 19, No. 1, 2007, pp. 012104-012104-15.
doi:10.1063/1.2434799

[17] G. Gordon, "Mechanism and Speed of Breakup of Drops," *Journal of Applied Physics*, Vol. 30, No. 11, 1959, pp. 1759-1761.
doi:10.1063/1.1735050

[18] F. Haas, "Stability of Droplets Suddenly Exposed to a High Velocity Gas Stream," *AIChE Journal*, Vol. 10, No. 6, 1964, pp. 920-924.
doi:10.1002/aic.690100627

[19] J. Hinze, "Fundamentals of the Hydrodynamic Mechanism of Splitting in Dispersion Processes," *AIChE Journal*, Vol. 1, No. 3, 1955, pp. 289-295.
doi:10.1002/aic.690010303

[20] S. Mehrota, "Mathematical Modeling of Gas Atomization Process for Metal Powder Production," Powder Metallurgy International, Vol. 13, No. 2, 1998, pp. 80-84.

[21] M. Gorokhovski and M. Herrmann, "Modeling Primary Atomization," *Annual Review of Fluid Mechanics*, Vol. 40, No. 1, 2008, pp. 343-366.
doi:10.1146/annurev.fluid.40.111406.102200

[22] H. P. Trinh, C. P. Chen and M. S. Balasubramanyam, "Numerical Simulation of Liquid Jet Atomization Including Turbulence Effects," *Journal of Engineering for Gas Turbines and Power*, Vol. 129, No. 4, 2007, pp. 920-928.

[23] J. Ishimoto, K. Ohira, K. Okabayashi and K. Chitose, "Integrated Numerical Prediction of Atomization Process of Liquid Hydrogen Jet," *Cryogenics*, Vol. 48, No. 5-6, 2008, pp. 238-247.
doi:10.1016/j.cryogenics.2008.03.006

[24] K. Pougatcha, M. Salcudeana, E. Chanb and B. Knapper, "A Two-Fluid Model of Gas-Assisted Atomization Including Flow through the Nozzle, Phase Inversion, and Spray Dispersion," *International Journal of Multiphase Flow*, Vol. 35, No. 7, 2009, pp. 661-675.
doi:10.1016/j.ijmultiphaseflow.2009.03.001

[25] G. S. E. Antipas, "Modeling of the Break up Mechanism in Gas Atomization of Liquid Metals, Part I. The Surface Wave Formation Model," *Computational Materials Science*, Vol. 35, No. 4, 2006, pp. 416-422.
doi:10.1016/j.commatsci.2005.03.009

[26] D. Bradley, "On the Atomization of Liquids by High-Velocity Gases," *Journal of Physics D*: *Applied Physics*, Vol. 6, No. 14, 1973, pp. 1724-1736.
doi:10.1088/0022-3727/6/14/309

[27] N. Dombrowski and W. Johns, "The Aerodynamic Instability and Disintegration of Viscous Liquid Sheets," *Chemical Engineering Science*, Vol. 18, No. 3, 1963, pp. 203-214.
doi:10.1016/0009-2509(63)85005-8

[28] G. S. E. Antipas, "Modeling of the Break up Mechanism in Gas Atomization of Liquid Metals, Part II. The Gas Flow Model," *Computational Materials Science*, Vol. 46, No. 4, 2009, pp. 955-959.
doi:10.1016/j.commatsci.2009.04.046

[29] G. Antipas, C. Lekakou and P. Tsakiropoulos, "The Break up of Melt Streams by High Pressure Gases in Spray Forming," *Proceedings of the Second International Conference on Spray Forming*, Swansea, 1993, pp. 15-24.

